Stromal and Endothelial Transcriptional Changes during progression from MGUS to Myeloma and after Treatment Response

Itziar Cenzano[1,2,*], Miguel Cócera[1,3,*], Marta Larrayoz[1], Lorea Campos-Dopazo[1], Sonia Sanz[1], Azari Bantan[2], Amaia Vilas-Zornoza[1,3], Patxi San-Martin[1], Paula Aguirre-Ruiz[1], Diego Alignani[1,3], Aitziber Lopez[1], Ignacio Sancho González[4,5], Javier Ruiz[5], Purificacion Ripalda-Cemborain[1], Marta Abengozar-Muela[6], Emma Muiños-López[1], Vincenzo Lagani[2,7,8], Jesper Tegner[2,9,10,11], Mikel Hernáez[3,12], Xabier Agirre[1,3], Benjamin Ebert[13], Bruno Paiva[1,3], Paula Rodriguez-Otero[3,14], Luis-Esteban Tamariz-Amador[3,14], Jesús San-Miguel[3,14], Borja Saez[1], José A. Martinez-Climent[1,3], Isabel A. Calvo[1,3,§], David Gomez-Cabrero[2,15,§], Felipe Prosper[1,3,14,§]

[1]Hematology and Oncology Program, Centre for Applied Medical Research (CIMA), Instituto de Investigaciones Sanitarias de Navarra (IdiSNA), Cancer Center Clinica Universidad de Navarra (CCUN), Pamplona, Spain.
[2]Bioscience Program, Biological and Environmental Sciences and Engineering Division (BESE), King Abdullah University of Science and Technology (KAUST), Thuwal, Saudi Arabia.
[3]Centro de Investigacion Biomedica en Red de Cancer (CIBERONC). Madrid, Spain.
[4]Hospital Reina Sofia de Tudela, Tudela, Spain.
[5]Hospital Universitario de Navarra, Instituto de Investigaciones Sanitarias de Navarra (IdiSNA), Pamplona, Spain.
[6]Departament of Pathology, Clinica Universidad de Navarra, Pamplona, Spain.
[7]SDAIA-KAUST Center of Excellence in Data Science and Artificial Intelligence, Thuwal, Saudi Arabia.
[8]Institute of Chemical Biology, Ilia State University, Tbilisi, Georgia.
[9]Computer Science Program, Electrical and Mathematical Sciences and Engineering Division, King Abdullah University of Science and Technology (KAUST), Thuwal, Saudi Arabia.
[10]Unit of Computational Medicine, Department of Medicine, Center for Molecular Medicine, Karolinska Institutet, Karolinska University Hospital, Stockholm, Sweden.
[11]Science for Life Laboratory, Solna, Sweden.
[12]Computational Biology Program. Cima Universidad de Navarra, Data Science and Artificial Intelligence Institute (DATAI) Universidad de Navarra, Instituto de Investigaciones Sanitarias de Navarra (IdiSNA). Pamplona, Spain.
[13]Department of Medical Oncology, Dana-Farber Cancer Institute, Harvard Medical School, Boston, United States of America.
[14]Hematology and Cell Therapy Department. Cancer Center Clinica Universidad de Navarra (CCUN), Instituto de Investigaciones Sanitarias de Navarra (IdiSNA). Pamplona, Spain.
[15]Translational Bioinformatics Unit, Navarrabiomed, Universidad Pública de Navarra (UPNA).

*These authors contributed equally to this work
[§]These authors jointly supervised this work

RUNNING TITLE: scRNA-seq of EC and MSC in MM progression and treatment

KEYWORDS
Multiple myeloma, MGUS, single-cell RNA sequencing, Endothelial cells, Stromal cells, tumor microenvironment, mouse models and VRd treatment

CORRESPONDING AUTHOR
Felipe Prósper (fprosper@unav.es), David Gomez-Cabrero (david.gomezcabrero@kaust.edu.sa) and Isabel A. Calvo (icalvoa@unav.es).

For original data, please contact (icenzano@unav.es)

ABSTRACT

The role of the bone marrow non-immune microenvironment (BME) in the transition from monoclonal gammopathy of undetermined significance (MGUS) into clinically active multiple myeloma (MM) remains incompletely defined. To address this, we performed single-cell RNA sequencing (scRNA-seq) of non-hematopoietic BME cells and MM cells from two genetically engineered mouse models ($BI_{c\gamma1}$ and $MI_{c\gamma1}$) that recapitulate MGUS to MM progression. Our analysis revealed distinct transcriptional trajectories in endothelial cells (EC) and mesenchymal stem cells (MSC), uncovering stage-specific BME–PC interactions that shape disease progression. EC adopted a stress phenotype during MGUS and transitioned into a proliferative, angiogenic state in MM. In parallel, MSC exhibited impaired differentiation capacity and an inflammatory transcriptional program that intensified during MM development. Notably, an interferon (IFN)-associated MM signature was detected in both EC and MSC from the $BI_{c\gamma1}$ model but was absent in the more aggressive $MI_{c\gamma1}$ model. We further show that treatment with bortezomib, lenalidomide, and dexamethasone (VRd) remodeled the BME by suppressing IFN-driven transcriptional programs, promoting an adaptive stress response in EC, and restoring osteogenic potential in MSC—shifting the niche toward a less tumor-permissive state. Importantly, elements of the IFN-related MM signature were validated in MSCs from newly diagnosed patients across the MGUS-to-MM spectrum, supporting the translational relevance of our findings. Together, these data define dynamic, targetable alterations in the non-immune BME during myeloma progression and highlight potential therapeutic strategies.

KEY POINTS

- EC and MSC undergo distinct transcriptional reprogramming during disease progression, with a coordinated IFN signature emerging in MM.
- VRd therapy reshapes the bone marrow niche by repressing IFN signaling, decreasing EC stress, and restoring MSC osteogenic function.

INTRODUCTION

Multiple myeloma (MM) is a B-cell malignancy characterized by the clonal expansion of plasma cells (PC) in the bone marrow (BM), preceded by asymptomatic precursor stages: monoclonal gammopathy of undetermined significance (MGUS) and smoldering multiple myeloma (SMM)[1]. Understanding the molecular mechanisms driving disease progression is crucial for developing therapies to prevent symptomatic MM.

The BM microenvironment (BME) comprises a complex network of hematopoietic and non-hematopoietic cells, extracellular matrix components, and soluble factors. This microenvironment creates an immunosuppressive and proinflammatory milieu that supports malignant PC growth and survival[2]. Therefore, the intricate interactions between myeloma cells and their surrounding microenvironment are crucial for developing effective therapies that can disrupt supportive signals and overcome drug resistance. While most studies have focused on the immune component[3–6], increasing evidence suggests that endothelial cells (EC) and mesenchymal stem cells (MSC) foster myeloma PC[7,8]. Furthermore, an enhanced inflammatory signature has been identified in MSC of MM patients[9–11]. However, the role of the non-hematopoietic BME to MGUS-to-MM progression remains poorly understood.

In this study, we took advantage of our recently described mouse models of MM that recapitulate the clinical, genetic, molecular, and immunological characteristics of MM patients[12]. These models include a precursor stage like MGUS that progresses into asymptomatic MM. Using single-cell RNA sequencing (scRNA-seq) data of Fluorescent-Activated Cell Sorted (FACS) non-hematopoietic BME cells and PC, we analyzed the transcriptional changes during the disease transition and in response to current therapy. Our results identified distinct transcriptional dynamics between EC and MSC at the different stages of the disease. EC exhibited an altered vascular profile at MGUS, followed by the upregulation of angiogenesis and proliferation pathways during MM. In contrast, MSC exhibited early inflammatory activation at the MGUS stage and downregulation of pathways associated with adhesion, osteogenic, and myogenic differentiation. Interestingly, we identified an interferon (IFN)- related myeloma signature in both EC and MSC within the slow-progression model that was reversed after treatment with VRd (bortezomib, lenalidomide, and dexamethasone). Changes were validated in MSC from patients with MGUS, SMM, and MM, highlighting their potential role in disease progression.

METHODS

All detailed information is provided in the supplemental methods.

Mice

We used two genetically engineered MM mouse models, $BI_{c\gamma1}$ and $MI_{c1\gamma}$, that recapitulate the common features observed in human MM. $YFP_{c\gamma1}$ mice were used as controls[12] (**Supplemental Table 1**). For each scRNA-seq experiment at MGUS and MM-like stages, we used a pool of BM cells from 5-6 mice. In $BI_{c\gamma1}$ mice with a humanized cereblon (CRBN)[13], VRd therapy was administered intraperitoneally for 20 consecutive weeks. The study included mice of both sexes and was approved by the Ethical Committee of Animal Experimentation of the University of Navarra and the Health Department of the Navarra Government.

Murine BM non-hematopoietic cells were isolated as previously described[14] and sorted as GFP-positive (GFP^+) PC using BD FACSAria II for subsequent scRNA-seq.

Human

BM aspirates from individuals of both sexes with newly diagnosed MGUS (n=5), SMM (n=2), or MM (n=10), and bone-chip BM samples from healthy donors (HD) (50-80 years of age) HD (n=8) undergoing orthopedic surgery were collected for bulk RNA-seq analysis. Immunofluorescence (IF) staining was performed on human BM biopsies from MGUS (n=4) and MM (n=7) patients, as well as on bone chips from HD (n=2). Written informed consent was obtained according to the Declaration of Helsinki and the

Institutional Review Board of the University of Navarra. The clinical characteristics of all individuals are described in **Supplemental Table 2**.

Samples were processed and BM cells were cryopreserved with FBS and 10% dimethyl sulfoxide (Sigma) in liquid nitrogen until use. Frozen samples were thawed, and MSC were prospectively isolated and stored at -80ºC for Bulk RNA sequencing (bulk RNA-seq).

Single-cell RNA and Bulk RNA sequencing

Details on library preparation, sequencing, and additional information, including quality control, differential expression analysis (DEA), gene ontology (GO) over-representation analysis (ORA), gene set enrichment analysis (GSEA), cell-cell communication, and gene regulatory network (GRN) analysis, are described in supplemental Methods.

RESULTS

Single-cell transcriptomic profiling of BM murine cells in control, MGUS, and MM

Using the $BI_{c\gamma1}$ myeloma model[12], we aimed to characterize the influence of the stromal and endothelial BME on disease transformation. This model, which carries BCL2 and $IKK2^{NF\text{-}\kappa B}$ genetic lesions triggered in germinal center B cells by a cre-cγ1 allele, develops signs of MGUS around 6 months of age that progressively transit into MM in 4 to 6 months later. Considering that $BI_{c\gamma1}$ mice received T-cell-driven immunization to drive PC formation, we included similarly immunized $YFP_{c\gamma1}$ mice, carrying a yellow-fluorescence reporter activated from germinal-center B cells, as controls (**Figure 1A**). We performed scRNA-seq on FACS-sorted non-hematopoietic BME cells (Lin^-, $TER119^-$, $CD45^-$, VDO^+, and $7AAD^-$) and PC (VDO^+, $7AAD^-$ and GFP^+) (**supplemental Figure 1**), yielding 12.437 cells (control=2.416, MGUS=4.169, MM=5.852). We identified 17 clusters comprising EC, MSC, PC, and other immune cells from the BME (**Figure 1B**; **supplemental Figure 2A-B**). Clusters were labeled using canonical markers (**Figure 1C; supplemental Figure 2C, D, E**). As a result eight clusters were labeled as PC (clusters PC1-8; n=7.924; markers: *Sdc1*, *Xbp1*, *Tnfrsf17*, and *Slamf7*); two clusters as erythroblasts (Erythro1-2; n=457; *Hba-a1*, *Hba-a2*, *Car1*, and *Car2*); one cluster as neutrophils (n=176; *S100a8*, *S100a9*, *Fcer1g*, and *Lyz2*); three clusters as EC (EC1-3; n= 3.288; *Cdh5*, *Cav1*, *Ly6c1*, and *Kdr*); and two clusters as MSC (MSC1-2; n= 592; mesenchymal and osteolineage-primed markers *Cxcl12*, *Pdgfra*, *Lepr*, and *Col1a2*).

To better understand the role of MSC and EC in MM progression, these two cell populations were analyzed separately (**supplemental Figures 2F-I)**. An increase in the number of BM EC was observed during MM development, which was validated by flow cytometry analysis (**Figures 1D-E; supplemental Figure 3**). Overall, these results support our cell enrichment strategy for isolating EC and MSC within the non-hematopoietic BME.

Identification of a MM-specific IFN signature in the BME

The increased EC numbers during MM suggested a connection with disease progression. Delving into the composition of EC, our analysis revealed a cluster of cells shared across all stages alongside a second cluster ("MM2") that was nearly unique to the MM stage, suggesting a role of the "MM2" cluster in MM (**Figure 2A**). The "MM2" cluster was characterized by the expression of IFN-inducible genes such as *Ifit2*, *Rsad2*, *Ifit3*, *Isg15*, *Ifi44*, *Ifit*, and *Oasl2*, indicating an upregulation of an IFN response, as supported by GO terms from GSEA (**Figure 2B, C**).

To uncover the mechanisms governing the IFN-like signature, we performed GRN analysis using SCENIC[15]. The study identified Irf7, Stat1, and Stat2 as master regulators significantly activated in "MM2" EC, with many target genes linked to T-cell regulation (**Figure 2D; supplemental Figure 4A-C**). These TFs are positive regulators of type 1 and type II IFN responses, which are associated with T cell immunosuppressive function in MM patients[16].

To determine whether the IFN-like signature was unique for EC, we evaluated the signature score related to "MM2" EC across other BM cell populations. This signature was also significantly upregulated in MM MSC at the MM stage as well as PC, neutrophils, and erythroblasts, suggesting a shared immunomodulatory

response of the BME to the disease (**Figures 2E-F; supplemental Figure 4D**). As the signature was not present in control $YFP_{c\gamma1}$ mice or at precursor stages, we termed it MM-IFN signature to emphasize its association with the myeloma stage. Immunofluorescence (IF) staining of BM samples from Control mice ($YFP_{c\gamma1}$) and $BI_{c\gamma1}$ mice at MGUS and MM stages, validated the increased proportion of IFN^+ EC and MSC in the MM stage (**Figures 2G-I; supplemental Figure 4E)**.

Interestingly, when the MM-IFN signature was analyzed in the $MI_{c\gamma1}$ model[12], which carries MYC and $IKK2^{NF\text{-}\kappa B}$ expression from germinal-center B cells, no significant enrichment at any stage in either population was observed (**supplemental Figure 4F-I).** This finding prompted us to investigate this MM-IFN signature in patients. The analysis of a publicly available dataset containing MSC from MM patients and healthy donors (HD)[10] uncovered an enrichment of the murine MM-IFN signature in a subset of MM patients, which was observed independently of genomic alterations (**supplemental Figure 4J-K**). Collectively, our findings suggest that IFN-signaling is a coordinated response within the BME that could define a subgroup of MM patients.

A stress pre-vascular state characterizes EC during the MGUS stage

To investigate deeper the molecular mechanisms of myeloma progression, we analyzed the transcriptional changes among the non-IFN EC at the different stages of the disease. An initial analysis uncovered a distinct transcriptome profile of EC at the MGUS stage (**Figure 3A**). Remarkably, MGUS EC overexpressed *Slpi*, *Hspa5*, *Mt1* and *Mt2*, indicating a stress state at the onset of the disease related to protein folding, reticulum stress, and ion homeostasis (**Figure 3B; supplemental Figure 5A-B; supplemental Table 3**). The upregulation of these genes may represent a "pre-vascular phase" in the progression to MM[17]. Moreover, *Cd74*, *Tmem176a*, and *Nme2*, which are involved in various pathological conditions[18–20], were also overexpressed in MGUS EC (**supplemental Figure 5C**).

Differential expression analysis (DEA) between MGUS and MM EC identified 180 differentially expressed genes (DEGs) (175 upregulated and 5 downregulated) (**Figure 3C; supplemental Table 4**), with MM EC showing a pro-vascular and lipid metabolism signature (**Figure 3D**). Notably, *Sox18*, key to tumor vascular development[21], was upregulated. (**supplemental Figure 5D**).

In the MIcγ1 model, we observed a stress-related transitional state like BIcγ1. MGUS EC expressed genes typical of MM EC, indicating a stronger vascular phenotype and faster progression (**supplemental Figure 6A–F**).

Next, we examined deregulated regulons between MGUS and MM non-IFN EC of the $BI_{c\gamma1}$ model, which better mimics the slower progression observed in humans. The analysis revealed a decline in the activity of regulons during disease progression (**Figure 3E; supplemental Figure 7A-B**). Xbp1, promoting endothelial proliferation via VEGF [22], showed the highest activity in MGUS EC (**Figure 3F; supplemental Figure 7B-C**), while Fos regulon was active at both stages, indicating its sustained role in both PC and BM EC[23] (**supplemental Figure 7C**). Interestingly, Sox18 regulon activity recovered in MM, suggesting involvement in pathogenesis (**Figure 3F; supplemental Figure 7C**). Globally, these findings reveal that MM-associated vascularization is preceded by a stress-related regulatory state in MGUS EC, potentially contributing to disease progression.

MSC undergo early transcriptional changes during pre-malignant MGUS that persist in symptomatic MM

DEA indicated that MSC deregulation begins at the MGUS stage (**Figure 4A**). GSEA revealed impaired osteogenic and adipogenic differentiation capacity in MSC during MM development, consistent with prior studies[8,9,24] (**Figure 4B; supplemental Table 5**). Additionally, we identified downregulation of muscle development genes, including *Pi16*, *Myl6*, *Enpp2*, *Nupr1*, and *Shox2*, which were not previously linked to MM.

Given early changes at the MGUS stage, we compared MGUS and control MSC, identifying 409 DEGs (**supplemental Table 6**). MGUS MSC exhibited enhanced expression of genes and pathways related to oxidative phosphorylation, ATP metabolism, protein folding, and RNA processing (**Figure 4C-D**). Upregulation of *Cd74* in MGUS MSC and EC suggests its potential role in MM progression. Comparatively,

only 35 DEGs were identified between MM and MGUS MSC (21 upregulated and 14 downregulated), mainly related to immune response, consistent with the inflammatory profile in human MM MSC[10] (**Figure 4E-G; supplemental Table 7).** Similar transcriptional changes were observed in MIcγ1 mice, reinforcing impaired differentiation during MM development (**supplemental Figure 8**).

Finally, the regulon analysis identified key transcription factors driving MSC alterations during MM progression (**Figure 4H; supplemental Figure 9A**). Control MSC were enriched in Sp7, Dlx5, Sox8, Sox9, and Cebpa, well-known TFs mediating osteochondrogenic and adipogenic differentiation. Reduced Klf4 activity supported impaired myogenic potential in MGUS and MM MSC. Moreover, TFs from the AP-1 family and Egr1 showed the highest regulon activity in MGUS MSC, aligning with their implication in MM development[25,26]. Yy1 and Xbp1 regulons remained active from MGUS to MM, while Elk3 was specific to MM, suggesting a more invasive role[27–29] (**supplemental Figure 9B-C**). Overall, our results suggest that MSC undergo a transcriptional shift at the MGUS stage that persists through disease progression.

Altered crosstalk between EC and MSC with malignant PC is potentially associated with myeloma development

To further understand the mechanism underlying BME-PC communication and how they change upon disease progression, we analyzed cellular communication through LIANA ligand-receptor (L-R) analysis[30] (**Figure 5**). Focusing on EC-PC communication, the number of interactions decreased during the MGUS stage, and increased in MM (**Figure 5A, supplemental Figure 10A; supplemental Table 8**). Interactions, through the *Fn1* ligand and *Insr* receptor in EC and the *Cd93* PC receptor, were identified only in controls, while *Apoe* ligand in EC and *Adam9*, *C3*, and *Vegfa* PC ligands were only found in MM (**Figure 5B**). Our results support the role of angiogenesis in myeloma via *Vegfa* secretion from PC, interacting with *Kdr*, *Nrp1*, and *Nrp2* in EC. High expression of Nrps has been correlated with poor outcomes in multiple cancers[31]. In addition, *Efna1-Epha8* interaction was predicted exclusively in MM (**Figure 5B; supplemental Figure 10B**).

Interestingly, MSC-PC interactions declined along disease progression (**Figure 5A; supplemental Figure 10C; supplemental Table 9**). We observed a decrease of *Thbs1-Itga4* and *Thbs2-Itga4* interactions that may be related to malignant PC extravasation (**Figure 5C**). MGUS and MM PC participate in outgoing interactions involving *Mfge8* and *Sdc3*-mediated incoming interactions not predicted in controls (**Figure 5C**). Further analysis of cellular communication revealed interactions related to cell motility and adhesion in MM (**supplemental Figure 10D**). Likewise, *Adam9*, which promotes cancer egress and invasion[32], interacts with MSC through *Itgav* and *Itgb1* in MM (**Figure 5C)**.

We uncovered common L-R pairs between EC-PC and MSC-PC along disease progression (**Figure 5D**). Multiple interactions via the *Itgb5* PC receptor were initiated during MGUS. Moreover, malignant PC interacted with MSC and EC through *Vegfa* secretion, highlighting the role of angiogenesis in MM. Additionally, *C3*-mediated interactions between PC and the non-hematopoietic BME in MM suggest that *C3* crosstalk maintains the immunosuppressive environment. Overall, identifying stage-specific BME-PC interactions should improve the understanding of MM development.

Single-cell RNA sequencing reveals VRd-induced EC and MSC remodeling in myeloma mice

To assess the impact of MM therapy on EC and MSC molecular signatures, we performed scRNA-seq on $BI_{c\gamma1}$ mice carrying humanized $CRBN^{I391V}$ ($BI_{c\gamma1}$-$Crbn^{I391V}$)[13] after 20 weeks of treatment with standard of care bortezomib (Velcade®), lenalidomide (Revlimid®), and dexamethasone (VRd), administered once MM was present (**supplemental Figure 11A-C**). As expected, VRd treatment significantly reduced the tumor burden and improved survival outcomes (**supplemental Figure 11D-E**). Given the role of IFN signaling as a myeloma-specific response, we first sought to determine the presence of IFN signature after treatment. Interestingly, VRd therapy downregulated IFN-driven MM signaling in EC and other BM populations (**Figure 6A, supplemental Figure 11F**). As a result, EC from treated mice exhibited decreased expression of IFN-induced genes, such as *Ifit1*, *Ifit2*, *Gbp2*, and *Isg15*, and key related regulons previously upregulated during myeloma development (**supplemental Figure 11G, supplemental Table 10**). IF analysis further confirmed the decreased in IFN^+ EC and MSC following VRd treatment, supporting a potential link between IFN signaling suppression and the anti-myeloma drug response (**Figure 6B-D, supplemental Figure 11H)**.

Beyond dampening the IFN signature, VRd treatment induced broader gene expression changes in both EC and MSC. In EC, DEA revealed upregulation of genes involved in mitochondrial metabolism, stress response, detoxification, and chromatin remodeling—indicative of an adaptive response (**Figure 6E-F)**. Consistent with its known tumor-suppressive role and previous studies in MM cells after bortezomib exposure, *Klf2* was upregulated in VRd-treated EC[33,34] (**supplemental Figure 11I)**. Furthermore, GRN analysis revealed enhanced activity of Zbtb7a and Rarg regulons, reinforcing this adaptive response[35,36] (**supplemental Figure 11J)**. Treated EC were enriched in thrombotic regulation pathways, including upregulation of *Hmgb1*, a gene linked to MM drug resistance[37] (**supplemental Figure 11K**). In contrast, vascular and adhesion-related genes, including *Nrp1,* were downregulated, consistent with lenalidomide's anti-angiogenic effects[38,39] and reduced *Xbp1* and *Ets2* activity.

In MSC, VRd treatment downregulated immune and IFN signaling pathways, indicating reduced inflammation in the BME (**Figure 6G)**. Likewise, antigen presentation genes, such as *Cd74*, *B2m* and *Psmb8* were downregulated (**Figure 6H, supplemental Table 11)**. Interestingly, decreased expression of *Mdm4* and *Cyba* in treated MSC suggests that VRd may impair the proliferative supportive capacity of MSC[40,41] (**supplemental Figure 12A)**. On the contrary, genes linked to ECM organization, wound healing, and bone development were upregulated, aligning with bortezomib's anabolic effects[42,43] **(supplemental Figure 12B).** GRN analysis confirmed osteogenic reprogramming via reactivation of Cebpa, Nfib, Nfic, Churc1 and Sox4 regulons (**supplemental Figure 12C)**. Finally, MSC-PC communication analysis identified the reemergence of interactions previously observed in control MSC such as *Adam10–Tspan5*, *Adam17–Il6ra* and *Wnt10a–Fzd1/Lrp6* which may contribute to anti-inflammatory and osteogenic adaptations following VRd treatment[44–47] (**supplemental Figure 12D)**. Overall, our results suggest that VRd therapy suppresses IFN-driven MM signaling and reprograms the BM niche by triggering an adaptive stress response in EC and restoring MSC osteogenic potential, creating a less tumor-permissive BME.

Transcriptional dynamics of human MSC during myeloma progression

To validate mouse model findings, we performed bulk RNA-seq in FACS-isolated MSC from aged-matched HD (n=8), newly diagnosed MGUS (n=5), SMM (n=2), or MM (n=10) patients (**Figure 7A; supplemental Figure 13**). PCA revealed a distinction between MM-MSC and HD-MSC, with MGUS-MSC and SMM-MSC mapped between them, showing an evolving transcriptional trajectory (**Figure 7B**).

The comparison between MGUS-MSC and HD-MSC revealed 180 DEGs (120 upregulated and 60 downregulated) (**supplemental Figure 14A; supplemental Table 12**). Downregulated genes, such as *TNN, SPP1,* and *A2M,* were related to osteoblast differentiation. Besides, MGUS-MSC upregulated genes related to cell cycle, protein folding and ubiquitination (**supplemental Figure 14B**). Mitochondrial activity, ATP metabolism, and oxidative stress were also enriched in MGUS-MSC, as previously stated in our mouse data, reinforcing their role in MM pathogenesis.

Consistent with the high transcriptional similarity observed in mice, the fewest DEGs were yielded when comparing MGUS and MM MSC (41 upregulated and 33 downregulated) (**supplemental Figure 14C; supplemental Table 13**). MM-MSC showed enrichment in inflammatory-related processes, indicating that a pro-inflammatory microenvironment is required to transition from premalignant stages to active myeloma (**supplemental Figure 14D**). In addition, MM-MSC over-expressed *PHLDA1*, *FOXC2*, *PPA1*, and *CTNNB1*, genes associated with Epithelial-Mesenchymal Transition (EMT), which aligns with MSC potential to induce EMT through extracellular vesicles in more aggressive MM[48] (**supplemental Figure 14C-D)**.

Defective osteogenic differentiation and dysfunctional immunomodulatory ability were confirmed when comparing MM- vs HD-MSC (448 upregulated and 566 downregulated) (**Figure 7C, supplemental Figure 14E-F; supplemental Table 14)**. Furthermore, consistent with the impaired myogenic phenotype observed in mice, human MM-MSC showed downregulation of muscle-related genes (**supplemental Figure 14F**). GSEA revealed enrichment of TNF-α signaling via NF-KB and IFN response in MM-MSC (**Figure 7D)**. Interestingly, the IFN signature previously identified in murine MM BME was enriched in a subset of MM patients, independent of genetic alterations (**Figure 7E, supplemental Figure 14G**). IF staining of BM

samples from MGUS and MM patients further confirmed the enrichment of IFN-driven MM signaling in MSC from a subset of MM patients (**Figure 7F-H, supplemental Figure 15A-B)**.

Finally, we determine the changes in regulon activity during myeloma progression (**Figure 7I**). MM-MSC exhibited increased activity of TF related to the NF-KB pathway, IRF1 and IRF3, which again emphasizes the importance of IFN signaling for the disease. In conclusion, the transcriptional reprogramming of MSC along the disease continuum supports a consistent pattern shared in human patients and mouse models.

DISCUSSION

Over the last decades, our understanding of MM biology has advanced significantly [49–53], explicitly revealing the contribution of the BME to the outgrowth and relapse of this neoplasia and exerting a supportive function for the expansion of malignant PC[3,10,54–56]. However, research has mainly concentrated on PC and their immune microenvironment, highlighting the need for additional exploration of the non-hematopoietic BME[57–60]. Here, using our $BI_{c\gamma1}$ and $MI_{c\gamma1}$ murine models[12], we provided a comprehensive overview of transcriptional deregulation within EC and MSC during the transition from healthy to MGUS and MM, and a BME reshaping in response to VRd treatment. Moreover, we analyze the translational relevance of these findings in MSC from MM patients at various stages of the disease.

Our study identifies a myeloma-specific IFN signature in EC that extends to MSC and other BM cells, indicating a shared BME response during MM progression. This signature, marked by upregulation of IFN-inducible genes and master regulators (Irf7, Stat1, Stat2), is suppressed following VRd treatment, shifting the BME toward a less tumor-permissive state. STAT1/2 signaling, closely linked to IFN in MM, supports tumor-promoting roles, complementing *STAT3*'s known oncogenic function and role in MM migration and BM homing[61]. While prior scRNA-seq studies reported IFN activity in PC and immune cells[3,4], only limited evidence suggested an IFNα response in MSC[57,60]. This IFN-inducible response reveals an immunomodulatory role of the non-hematopoietic BME, with EC and MSC contributing to immune remodeling and T-cell exhaustion in inflammatory conditions[16]. The enrichment of this IFN signature in MSC from a subset of MM patients highlights its clinical relevance for patient stratification based on inflammatory features.

Non-IFN EC in MGUS exhibited transcriptional changes linked to protein folding and ion homeostasis, with upregulation of *Slpi*, *Mt1*, *Mt2*, and *Hspa5*, known for their roles in tumor angiogenesis and pro-survival signaling[62,63], potentially serving as early myeloma markers in EC. Disease progression from MGUS to MM in EC involved angiogenesis, migration, and metabolic shifts, with *Sox18* upregulation, a key regulator of vascular development and cancer progression[21], highlighting its potential as a disease target.

Unlike EC, MSC showed early transcriptional alterations in MGUS, including impaired osteogenic/adipogenic differentiation and a metabolic shift that supports MM progression[8,9]. The enrichment of cytokines TNFα, and NF-κB pathways promotes a pro-inflammatory niche[10], while upregulated type I IFN signaling reinforces disease advancement. Key regulators such as *Egr1*, AP-1 TFs, and *Elk3* drive MSC reprogramming, highlighting their potential as biomarkers and therapeutic targets.

Understanding the crosstalk between the BME and PC is crucial for unraveling tumor progression mechanisms, and this study represents the first investigation into the interactions between EC, MSC, and malignant PC along the disease evolution. As MM progresses, EC-PC communication declines in MGUS and restores in MM, highlighting their evolving relationship. *Vegfa* secretion from PC and its interaction with *Kdr*, *Nrp1*, and *Nrp2* endothelial receptors underscores angiogenesis as a hallmark of MM. Additionally, identifying *Efna1-Epha8* interaction exclusively in MM implicates the ephrin pathway in disease development, as previously described in other cancers[64]. Remarkably, MSC-PC interactions were linked to adhesion, matrix organization, and migration, suggesting MSC-PC crosstalk is crucial for MM extravasation and disease dissemination.

Despite effective treatments for newly diagnosed MM, relapse remains a challenge. Understanding treatment response mechanisms can enhance immunotherapy and accelerate a cure. Combinatorial regimens, like VRd,

improve outcomes by targeting multiple pathways, modulating immune cells, inhibiting myeloma growth, and reshaping the BME[65,66]. Using our MGUS-MM mouse models, we demonstrate for the first time that MM treatment impacts the non-hematopoietic BME by suppressing IFN signaling, inducing adaptive stress in EC, and restoring MSC osteogenic potential, shifting the niche toward a less tumor-permissive state. These findings highlight the importance of targeting BME interactions and enhancing anti-myeloma immune responses.

Challenges associated with the BM EC and stromal isolation hinder human scRNA-seq studies. Our bulk RNA-seq showed impaired MSC differentiation in human patients, consistent with murine findings, even at premalignant stages. Similarly, MGUS prompted a metabolic swift in human MSC with increased protein folding. Human MM-MSC exhibited higher expression of inflammation-related genes, potentially aiding in the immune evasion of MM by suppressing T cells, which could be enhanced by overexpressing *LGALS9* or *FADD*[67,68]. On the contrary, discrepancies in matrix-related genes (*SDC2*, *SDC4*, *MMP14*, and *LAMC1*), between species may reflect MM patient heterogeneity and clinical variability. Notably, these genes were linked to patients with poor outcomes and may not fully align with the $BI_{c\gamma1}$ mouse model.

In summary, the use of the $BI_{c\gamma1}$ myeloma murine model, which mimics MGUS-to-MM progression, alongside scRNA-seq, has enabled a comprehensive dissection of the non-hematopoietic BME. The myeloma-specific IFN signature, the transition stress state in MGUS EC, the early transcriptional shifts in MSC, the evolving cellular communication networks and the IFN signaling repression post-VRd therapy collectively reinforce the role of EC and MSC in MM development and treatment response. Validation in human patients reinforces the study's translational relevance, suggesting that non-hematopoietic BME changes may foster MM development from premalignant stages and shift toward a less tumor-permissive state after treatment.

ACKNOWLEDGEMENTS
This work was supported by the Instituto de Salud Carlos III and co-financed by ERDF A way of making Europe (PI20/01308, PI22/00983, PI23/00516); CIBERONC (CB16/12/00489), RICORS TERAV (RD21/0017/0009); Departamento de Industria Gobierno de Navarra (AGATA 0011-1411-2020-000010/0011-1411-2020-000011) and Departamento de Salud Gobierno de Navarra; the Cancer Research UK [C355/A26819]; FC AECC and AIRC under the Accelerator Award Program; The International Myeloma Foundation (Brian van Novis) and The Paula and Rodger Riney Foundation to FP. The study was also supported by The Spanish Government, through project PID2019-111192GA-I00 (MICINN) to DGC. IAC was supported by Marie Curie grant (H2020-MSCA-IF-837491) from European Commission. IC was supported by AECC predoctoral fellowship (PRDNA19006CENZ). MC was supported by FPU fellowship (FPU22/03283) from Ministerio de Ciencia, Innovación y Universidades.

We would like to thank the staff of the flow cytometry core, the advanced genomic lab, and the animal facility at CIMA Universidad de Navarra for their invaluable technical and intellectual assistance. We also acknowledge Hospital Reina Sofía de Tudela, Hospital Universitario de Navarra, the Biobank of the University of Navarra, and Goretti Ariz for the provision of BM samples and their collaboration. We are particularly grateful to the patients and healthy donors for their participation in this study.

AUTHORSHIP CONTRIBUTIONS
I.C., M.C., L.C-D. and I.A.C. processed murine and human BM samples; B.S. and I.A.C. conceptualized the study and analyzed the scRNA-seq experiments data; I.C., M.C., and I.A.C. interpreted the scRNA-seq experiments data; I.C. and I.A.C. wrote the paper; M.C. analyzed the bulk RNA-seq experiments data; M.C. and I.A.C. interpreted the bulk RNA-seq experiments data; M.L. and J.A.M.C. designed and provided the mice models; M.L. and S.S. performed the VRd treatment experiments. A.B. performed the cell-cell computational analysis; A.V., P.S.M., and P.A.R. performed the scRNA-seq and bulk RNA-seq experiments. D.A. and A.L. performed the FACS sorting. I.S.G. and J.R. provided the BM samples from HD; M.C., L.C-D. and P.R-C. conducted the histologic experiments; M.C. analyzed the histologic experiments; M.A-M. and E.M. provided the human MGUS and MM samples. D.G.C., with help from M.H. and J.T., supervised the computational work. B.E. provided the humanized mouse model; B.P. and J.S-M. helped with the clinical data; P.R.O. and L.E.T-A. provided the BM samples from MGUS, SMM, and MM patients; I.A.C. and B.S. designed the research experiments; F.P., D.G.C. and I.A.C. conceived and directed the research project.

All authors actively participated in the discussions underlying this manuscript. I.C., M.C., I.A.C., D.G.C., and F.P. discussed the results and wrote the final manuscript. All authors contributed to, read, and approved the final manuscript.

DISCLOSURE OF CONFLICTS OF INTEREST
A patent on the knowhow and experimental use of the $BI_{c\gamma1}$ and $MI_{c\gamma1}$ mouse models of MM has been licensed to MIMO Biosciences. J.A.M.-C. has received research funding from Roche-Genentech, Bristol Myers Squibb, Janssen, Regeneron, Priothera Pharmaceuticals, Palleon Pharmaceuticals, AstraZeneca, and K36 Therapeutics, and is founder and holds stock options of MIMO Biosciences. The authors declare no competing interests.

REFERENCES

1. Kumar SK, Rajkumar V, Kyle RA, et al. Multiple myeloma. *Nat Rev Dis Primers*. 2017;3(1):17046.
2. Lomas OC, Tahri S, Ghobrial IM. The microenvironment in myeloma. *Curr Opin Oncol*. 2020;32(2):170–175.
3. Zavidij O, Haradhvala NJ, Mouhieddine TH, et al. Single-cell RNA sequencing reveals compromised immune microenvironment in precursor stages of multiple myeloma. *Nature Cancer 2020 1:5*. 2020;1(5):493–506.
4. Boiarsky R, Haradhvala NJ, Alberge JB, et al. Single cell characterization of myeloma and its precursor conditions reveals transcriptional signatures of early tumorigenesis. *Nature Communications 2022 13:1*. 2022;13(1):1–15.
5. Pilcher W, Thomas BE, Bhasin SS, et al. Cross center single-cell RNA sequencing study of the immune microenvironment in rapid progressing multiple myeloma. *npj Genomic Medicine 2023 8:1*. 2023;8(1):1–18.
6. Chen M, Wan Y, Li X, et al. Dynamic single-cell RNA-seq analysis reveals distinct tumor program associated with microenvironmental remodeling and drug sensitivity in multiple myeloma. *Cell Biosci*. 2023;13(1):1–18.
7. García-Ortiz A, Rodríguez-García Y, Encinas J, et al. The Role of Tumor Microenvironment in Multiple Myeloma Development and Progression. *Cancers (Basel)*. 2021;13(2):217.
8. Maiso P, Mogollón P, Ocio EM, Garayoa M. Bone Marrow Mesenchymal Stromal Cells in Multiple Myeloma: Their Role as Active Contributors to Myeloma Progression. *Cancers 2021, Vol. 13, Page 2542*. 2021;13(11):2542.
9. Alameda D, Saez B, Lara-Astiaso D, et al. Characterization of freshly isolated bone marrow mesenchymal stromal cells from healthy donors and patients with multiple myeloma: transcriptional modulation of the microenvironment. *Haematologica*. 2020;105(9):e470.
10. de Jong MME, Kellermayer Z, Papazian N, et al. The multiple myeloma microenvironment is defined by an inflammatory stromal cell landscape. *Nature Immunology 2021 22:6*. 2021;22(6):769–780.
11. de Jong MME, Fokkema C, Papazian N, et al. An IL-1β-driven neutrophil–stromal cell axis fosters a BAFF-rich protumor microenvironment in individuals with multiple myeloma. *Nature Immunology 2024*. 2024;1–14.
12. Larrayoz M, Garcia-Barchino MJ, Celay J, et al. Preclinical models for prediction of immunotherapy outcomes and immune evasion mechanisms in genetically heterogeneous multiple myeloma. *Nat Med*. 2023;29(3):632–645.
13. Fink EC, McConkey M, Adams DN, et al. Crbn I391V is sufficient to confer in vivo sensitivity to thalidomide and its derivatives in mice. *Blood*. 2018;132(14):1535–1544.
14. Ye J, Calvo IA, Cenzano I, et al. Deconvolution of the hematopoietic stem cell microenvironment reveals a high degree of specialization and conservation. *iScience*. 2022;25(5):104225.
15. Aibar S, González-Blas CB, Moerman T, et al. SCENIC: Single-cell regulatory network inference and clustering. *Nat Methods*. 2017;14(11):1083.
16. Sumida TS, Dulberg S, Schupp JC, et al. Type I interferon transcriptional network regulates expression of coinhibitory receptors in human T cells. *Nature Immunology 2022 23:4*. 2022;23(4):632–642.
17. Binet F, Sapieha P. ER Stress and Angiogenesis. *Cell Metab*. 2015;22(4):560–575.
18. Le Hiress M, Tu L, Ricard N, et al. Proinflammatory signature of the dysfunctional endothelium in pulmonary hypertension role of the macrophage migration inhibitory factor/CD74 complex. *Am J Respir Crit Care Med*. 2015;192(8):983–997.

19. Ye C, Ren S, Sadula A, et al. The expression characteristics of transmembrane protein genes in pancreatic ductal adenocarcinoma through comprehensive analysis of bulk and single-cell RNA sequence. *Front Oncol*. 2023;13:1047377.
20. Bai W, Wang H, Bai H. Identification of Candidate Genes and Therapeutic Agents for Light Chain Amyloidosis Based on Bioinformatics Approach. *Pharmgenomics Pers Med*. 2019;12:387.
21. Olbromski M, Podhorska-Okołów M, Dzięgiel P. Role of the SOX18 protein in neoplastic processes. *Oncol Lett*. 2018;16(2):1383.
22. Yang J, Xu J, Danniel M, et al. The interaction between XBP1 and eNOS contributes to endothelial cell migration. *Exp Cell Res*. 2018;363(2):262–270.
23. Jin Y, Chen K, De Paepe A, et al. Active enhancer and chromatin accessibility landscapes chart the regulatory network of primary multiple myeloma. *Blood*. 2018;131(19):2138–2150.
24. Fairfield H, Costa S, Falank C, et al. Multiple Myeloma Cells Alter Adipogenesis, Increase Senescence-Related and Inflammatory Gene Transcript Expression, and Alter Metabolism in Preadipocytes. *Front Oncol*. 2021;10:1.
25. Fan F, Podar K. The Role of AP-1 Transcription Factors in Plasma Cell Biology and Multiple Myeloma Pathophysiology. *Cancers (Basel)*. 2021;13(10):.
26. Chen L, Wang S, Zhou Y, et al. Identification of early growth response protein 1 (EGR-1) as a novel target for JUN-induced apoptosis in multiple myeloma. *Blood*. 2010;115(1):61–70.
27. Xu G, Liu K, Anderson J, et al. Expression of XBP1s in bone marrow stromal cells is critical for myeloma cell growth and osteoclast formation. *Blood*. 2012;119(18):4205.
28. Huerta-Yepez S, Liu H, Baritaki S, et al. Overexpression of Yin Yang 1 in bone marrow-derived human multiple myeloma and its clinical significance. *Int J Oncol*. 2014;45(3):1184–1192.
29. Lee M, Cho HJ, Park KS, Jung HY. ELK3 Controls Gastric Cancer Cell Migration and Invasion by Regulating ECM Remodeling-Related Genes. *Int J Mol Sci*. 2022;23(7):.
30. Dimitrov D, Türei D, Garrido-Rodriguez M, et al. Comparison of methods and resources for cell-cell communication inference from single-cell RNA-Seq data. *Nature Communications 2022 13:1*. 2022;13(1):1–13.
31. Benwell CJ, Johnson RT, Taylor JAGE, Price CA, Robinson SD. Endothelial VEGFR Coreceptors Neuropilin-1 and Neuropilin-2 Are Essential for Tumor Angiogenesis. *Cancer Research Communications*. 2022;2(12):1626–1640.
32. Fan X, Wang Y, Zhang C, et al. ADAM9 Expression Is Associate with Glioma Tumor Grade and Histological Type, and Acts as a Prognostic Factor in Lower-Grade Gliomas. *Int J Mol Sci*. 2016;17(9):.
33. Li YZ, Xie J, Wang RQ, et al. KLF2 is a clinical diagnostic and treatment biomarker of breast cancer. *Front Cell Dev Biol*. 2023;11:1182123.
34. Nayak L, Shi H, Atkins GB, et al. The thromboprotective effect of bortezomib is dependent on the transcription factor Kruppel-like factor 2 (KLF2). *Blood*. 2014;123(24):3828–3831.
35. Liu XS, Genet MD, Haines JE, et al. ZBTB7A suppresses melanoma metastasis by transcriptionally repressing MCAM. *Mol Cancer Res*. 2015;13(8):1206.
36. Xiu L, Zhao Y, Li N, et al. High expression of RARG accelerates ovarian cancer progression by regulating cell proliferation. *Front Oncol*. 2022;12:1063031.
37. De Stefano V, Larocca A, Carpenedo M, et al. Thrombosis in multiple myeloma: risk stratification, antithrombotic prophylaxis, and management of acute events. A consensus-based position paper from an ad hoc expert panel. *Haematologica*. 2022;107(11):2536.
38. Lu L, Payvandi F, Wu L, et al. The anti-cancer drug lenalidomide inhibits angiogenesis and metastasis via multiple inhibitory effects on endothelial cell function in normoxic and hypoxic conditions. *Microvasc Res*. 2009;77(2):78–86.

39. De Luisi A, Ferrucci A, Coluccia AML, et al. Lenalidomide restrains motility and overangiogenic potential of bone marrow endothelial cells in patients with active multiple myeloma. *Clinical Cancer Research*. 2011;17(7):1935–1946.
40. Marine J-C, Jochemsen AG, Lozano G, Levine AJ. MDMX (MDM4), a Promising Target for p53 Reactivation Therapy and Beyond. *Cold Spring Harb Perspect Med*. 2016;6(7):a026237.
41. Sarıman M, Abacı N, Ekmekçi SS, et al. Investigation of Gene Expressions of Myeloma Cells in the Bone Marrow of Multiple Myeloma Patients by Transcriptome Analysis. *Balkan Med J*. 2019;36(1):23–31.
42. Giuliani N, Morandi F, Tagliaferri S, et al. The proteasome inhibitor bortezomib affects osteoblast differentiation in vitro and in vivo in multiple myeloma patients. *Blood*. 2007;110(1):334–338.
43. Sekiguchi Y, Ichikawa K, Wakabayashi M, et al. Bone formation following lenalidomide-dexamethasone combination therapy in cases of multiple myeloma refractory to high-dose chemotherapy with bortezomib and autologous peripheral blood stem cell transplantation: report of a case and review of the literature. *Int J Clin Exp Pathol*. 2015;8(8):9609.
44. Schumacher N, Rose-John S. ADAM17 Activity and IL-6 Trans-Signaling in Inflammation and Cancer. *Cancers (Basel)*. 2019;11(11):1736.
45. Abdalla AME, Miao Y, Ming N, Ouyang C. ADAM10 modulates the efficacy of T-cell-mediated therapy in solid tumors. *Immunol Cell Biol*. 2024;102(10):907–923.
46. Liu J, Xiao Q, Xiao J, et al. Wnt/β-catenin signalling: function, biological mechanisms, and therapeutic opportunities. *Signal Transduction and Targeted Therapy 2021 7:1*. 2022;7(1):1–23.
47. Simic MK, Mohanty ST, Xiao Y, et al. Multi□Targeting DKK1 and LRP6 Prevents Bone Loss and Improves Fracture Resistance in Multiple Myeloma. *Journal of Bone and Mineral Research*. 2023;38(6):814.
48. Kletukhina S, Neustroeva O, James V, Rizvanov A, Gomzikova M. Role of Mesenchymal Stem Cell-Derived Extracellular Vesicles in Epithelial–Mesenchymal Transition. *Int J Mol Sci*. 2019;20(19):4813.
49. Cohen YC, Zada M, Wang SY, et al. Identification of resistance pathways and therapeutic targets in relapsed multiple myeloma patients through single-cell sequencing. *Nature Medicine 2021 27:3*. 2021;27(3):491–503.
50. Ledergor G, Weiner A, Zada M, et al. Single cell dissection of plasma cell heterogeneity in symptomatic and asymptomatic myeloma. *Nature Medicine 2018 24:12*. 2018;24(12):1867–1876.
51. Dutta AK, Alberge JB, Sklavenitis-Pistofidis R, et al. Single-cell profiling of tumour evolution in multiple myeloma — opportunities for precision medicine. *Nature Reviews Clinical Oncology 2022 19:4*. 2022;19(4):223–236.
52. Samur MK, Szalat R, Munshi NC. Single-cell profiling in multiple myeloma: insights, problems, and promises. *Blood*. 2023;142(4):313–324.
53. Tirier SM, Mallm JP, Steiger S, et al. Subclone-specific microenvironmental impact and drug response in refractory multiple myeloma revealed by single□cell transcriptomics. *Nature Communications 2021 12:1*. 2021;12(1):1–16.
54. Sharma NS, Choudhary B. Good Cop, Bad Cop: Profiling the Immune Landscape in Multiple Myeloma. *Biomolecules*. 2023;13(11):.
55. John L, Poos AM, Brobeil A, et al. Resolving the spatial architecture of myeloma and its microenvironment at the single-cell level. *Nature Communications 2023 14:1*. 2023;14(1):1–17.
56. Pilcher WC, Yao L, Gonzalez-Kozlova E, et al. A single-cell atlas characterizes dysregulation of the bone marrow immune microenvironment associated with outcomes in multiple myeloma. *bioRxiv*. 2024;2024.05.15.593193.

57. Kellermayer Z, Tahri S, de Jong MME, et al. Interferon gamma-mediated prevention of tumor progression in a mouse model of multiple myeloma. *Hemasphere*. 2024;8(12):.
58. de Jong MME, Chen L, Raaijmakers MHGP, Cupedo T. Bone marrow inflammation in haematological malignancies. *Nature Reviews Immunology 2024 24:8*. 2024;24(8):543–558.
59. Fotiou D, Katodritou E. From Biology to Clinical Practice: The Bone Marrow Microenvironment in Multiple Myeloma. *Journal of Clinical Medicine 2025, Vol. 14, Page 327*. 2025;14(2):327.
60. Ghamlouch H, Gagler DC, Blaney P, et al. A proinflammatory response and polarized differentiation of stromal elements characterizes the murine myeloma bone marrow niche. *Exp Hematol Oncol*. 2025;14(1):.
61. Chong PSY, Chng WJ, de Mel S. STAT3: A Promising Therapeutic Target in Multiple Myeloma. *Cancers (Basel)*. 2019;11(5):.
62. Zhu Y, Chang S, Liu J, Wang B. Identification of a novel cuproptosis-related gene signature for multiple myeloma diagnosis. *Immun Inflamm Dis*. 2023;11(11):e1058.
63. Si M, Lang J. The roles of metallothioneins in carcinogenesis. *J Hematol Oncol*. 2018;11(1):.
64. Pergaris A, Danas E, Goutas D, et al. The Clinical Impact of the EPH/Ephrin System in Cancer: Unwinding the Thread. *Int J Mol Sci*. 2021;22(16):.
65. Ho M, Xiao A, Yi D, Zanwar S, Bianchi G. Treating Multiple Myeloma in the Context of the Bone Marrow Microenvironment. *Current Oncology 2022, Vol. 29, Pages 8975-9005*. 2022;29(11):8975–9005.
66. Solimando AG, Krebs M, Desantis V, et al. Breaking through Multiple Myeloma: A Paradigm for a Comprehensive Tumor Ecosystem Targeting. *Biomedicines 2023, Vol. 11, Page 2087*. 2023;11(7):2087.
67. Akiyama K, Chen C, Wang D, et al. Mesenchymal-Stem-Cell-Induced Immunoregulation Involves FAS-Ligand-/FAS-Mediated T Cell Apoptosis. *Cell Stem Cell*. 2012;10(5):544–555.
68. Kim S, Lee H-J, Jeon M-S, Yi T, Song SU. Galectin-9 is Involved in Immunosuppression Mediated by Human Bone Marrow-derived Clonal Mesenchymal Stem Cells. *Immune Netw*. 2015;15(5):241.

FIGURE LEGENDS

Figure 1. Single-cell transcriptomic profiling of BM murine cells in control, MGUS, and MM. (A) Experiment overview. Schematic view of control ($YFP_{c\gamma1}$), $BI_{c\gamma1}$, and $MI_{c\gamma1}$ mice and experimental workflow for the isolation and scRNA-seq analysis of PC, MSC and EC. (B) Left panel: UMAP representation of murine BM microenvironment control, MGUS, and MM cells colored by cell clustering after merging samples. Right panels: Original UMAP split into control, MGUS, and MM datasets. (C) Dot plot of canonical markers used to define PC, EC, MSC, erythroblasts, and neutrophils. The dot size reflects the percentage of cells within the cluster expressing each gene, and the color represents the average expression level. (D-E) Left panel: UMAP projection showing the distribution of control, MGUS, and MM cells for EC (D) and MSC (E). Right panel: Bar plot depicting the total number of cells per stage for EC (D) and MSC (E).

Figure 2. Identification of a MM-specific IFN signature in the BME. (A) UMAP dimension reduction of EC revealing a transcriptionally distinct population in MM. (B) Dot plot visualization of the markers defining EC MM2 cluster. Average gene expression is shown by color intensity, and the percentage of cells expressing each gene is shown by size. (C) Bar charts of enriched Gene Ontology (GO) terms from GSEA (FDR < 0.05) computed using MM2 cluster markers. The horizontal axis represents the normalized enrichment score (NES). (D) Heatmap representing z-scaled mean regulon activity score of inferred top specific regulons for each stage. (E) UMAP plot illustrating the distribution of the IFN-related signature in EC across control, MGUS, and MM. (F) Violin plots showing AUC-score for IFN-related signature within EC in control, MGUS and MM cells. (G-H) Immunofluorescence (IF) staining of EC (Emcn, red), IFN response genes (Gbp2, yellow (G); Isg15, green (H)), and nucleus (DAPI) (blue) in Formalin-Fixed Paraffin-Embedded (FFPE) femurs from Control ($YFP_{c\gamma1}$), MGUS $BI_{c\gamma1}$ and MM $BI_{c\gamma1}$. (I) Quantification of the percentage of endothelial IFN-enriched cells, based on the coexpression of Emcn with IFN+ cells (Gbp2, (left plot); Isg15, (right plot)) in femurs from Control ($YFP_{c\gamma1}$), MGUS $BI_{c\gamma1}$ and MM $BI_{c\gamma1}$ mice.

Figure 3. A stress pre-vascular state characterizes EC during the MGUS stage. (A) Heatmap of the DEGs between control, MGUS, and MM cells. Color represents the z-score scaled expression values. (B) Violin plots showing the distribution of expression of genes upregulated in MGUS EC. (C) Volcano plot of the DEGs in MGUS vs. MM EC. The y-axis represents the -log10(p-value), and the x-axis represents the log2(fold change). The dot's color denotes the disease stage for which DEG was detected, with grey dots representing non-significant genes. (D) Significant terms derived from ORA between EC from MGUS and MM. (E) Heatmap representing z-scaled mean regulon activity score of inferred top specific regulons for EC in each stage. (F) Density plots showing the activity score of Xbp1 and Sox18 regulons in EC.

Figure 4. MSC undergo early transcriptional changes during pre-malignant MGUS that persist in symptomatic MM. (A) Heatmap depicting DEGs between MSC in control, MGUS, and MM. Color represents the z-score scaled expression values. (B) Heatmap of significantly downregulated GO terms in MGUS and MM cells compared to control MSC with the associated genes. The green color represents the presence of the gene in each GO term. (C) Volcano plot of the DEGs from the comparison between MSC from control and MGUS. The y-axis represents the -log10(p-value), and the x-axis represents the gene's log2(fold change). The dot's color denotes the disease stage for which DEG was detected, with grey dots representing non-significant genes. (D) Significant terms derived from ORA of MSC from control vs MGUS. (E) Volcano plot of the DEGs in MSC from MGUS vs. MM. (F) ORA between MSC from MGUS and MM. (G) GSEA plots for the gene sets 'TNFα signaling via NFκB' (left panel) and 'Interferon gamma response' (right panel) in MGUS vs MM MSC. (H) Heatmap of mean regulon activity score of significantly enriched regulons in each stage. The color scale represents the z-score of the activity scaled by row.

Figure 5. Altered crosstalk between EC and MSC with malignant PC is potentially associated with myeloma development (A) Heatmap showing the number of predicted cellular interactions between EC, MSC and PC. Block sizes and colors are proportional to the number of ligand-receptor pairs. (B-C) Dot plots of representative ligand-receptor interactions between PC and EC (B) or MSC (C) during disease progression. Dot size and color indicate the interaction's specificity and strength, respectively. (D) Chord

diagram showing a shared relevant signaling network between EC, MSC, and malignant PC in the MGUS and MM stages. Colors and width represent signal senders and strength, respectively.

Figure 6. Single-cell RNA sequencing reveals VRd-induced EC and MSC remodeling in myeloma mice.
(A) Violin plot showing AUC-score for IFN-related signature in EC from Control ($YFP_{c\gamma1}$), MM $BIc_{\gamma1}$ (MM) and MM $BI_{c\gamma1}$-*Crbn*^{I391V} VRd-treated (VRd) mice. (B-C) IF staining of EC (Emcn, red), IFN response genes (Gbp2 (yellow, (B)); Isg15 (green, (C)), and nucleus (DAPI) (blue) in FFPE femurs from MM $BI_{c\gamma1}$ mice (MM) and VRd-treated mice. (D) Quantification of the percentage of endothelial IFN^+ cells, determined by the coexpression of Emcn with IFN response genes (Gbp2 (upper plot) and Isg15 (bottom plot). (E) Heatmap showing the expression of stress-related DEGs identified in the comparison between treated and non-treated non-IFN MM EC at different stages of the disease. Color represents the z-score scaled expression values. (F) Significant terms derived from ORA between VRd-treated and untreated non-IFN MM EC. (G) Significant terms derived from ORA of MSC from MM mice before and after VRd treatment. (H) Heatmap projecting the expression of DEGs identified in the comparison between non-treated and treated MSC at different stages of the disease. Color represents the z-score scaled expression values.

Figure 7. Transcriptional dynamics of human MSC during myeloma progression. (A) An experimental workflow was used for the isolation and bulk RNA-seq analysis of human BM MSC. (B) PCA of MSC expression profiles shows clustering by disease stage. The color of the dots represents disease stages. (C) Heatmap showing the expression profiles across samples of DEGs identified in each pairwise comparison along disease progression. (D) GSEA plots for the gene sets 'TNFα signaling via NFκB' (left panel) and 'Interferon gamma response' (right panel) in the comparison between healthy donors (HD)- MSC and MM-MSC. (E) PCA plot showing the MM-IFN signature score in each human sample, previously identified murine BM MM cells. (F-G) IF staining of MSC (CD271, red), IFN response genes (*GBP2*, yellow (F); *ISG15*, green (G)), and nucleus (DAPI) (blue) in archived paraffined human BM biopsies of MM patients with low (MM LOW) and high IFN signal (MM HIGH) in stromal cells (see Supplementary Table 2). (H) Quantification of the percentage of mesenchymal IFN^+ cells, determined by the coexpression of CD271 with IFN response genes (*GBP2* (left plot), and *ISG15* (right plot)) in FFPE biopsies from HD (two donors) and archived paraffined human BM biopsies of MGUS (four patients) and MM patients (seven patients with low and high IFN signal in stromal cells). (I) Heatmap representing the variation of TF activity score across samples.

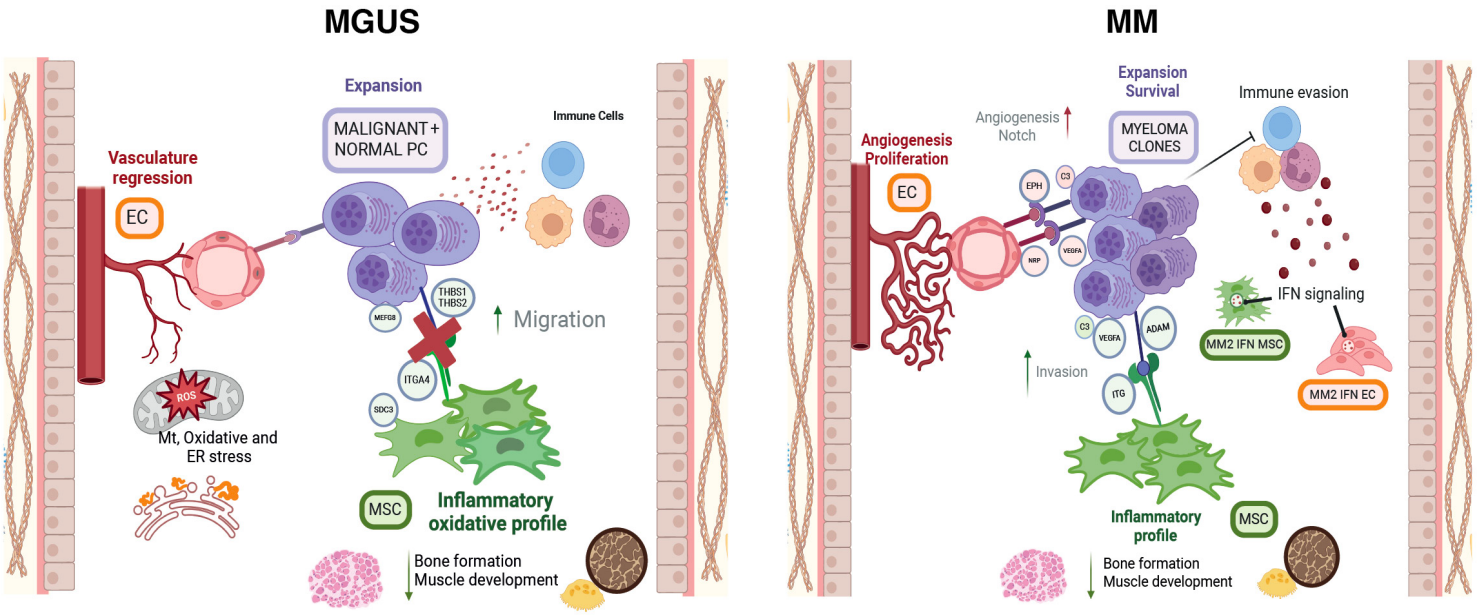
MGUS
Expansion
MALIGNANT + NORMAL PC
Immune Cells
Vasculature regression
EC
THBS1
THBS2
MEFG8
Migration
ITGA4
SDC3
ROS
Mt, Oxidative and ER stress
MSC
Inflammatory oxidative profile
Bone formation
Muscle development
MM
Expansion Survival
Immune evasion
Angiogenesis Notch
MYELOMA CLONES
Angiogenesis Proliferation
EC
EPH
C3
NRP
VEGFA
IFN signaling
MM2 IFN MSC
MM2 IFN EC
C3
VEGFA
ADAM
Invasion
ITG
Inflammatory profile
MSC
Bone formation
Muscle development

FIGURE 1

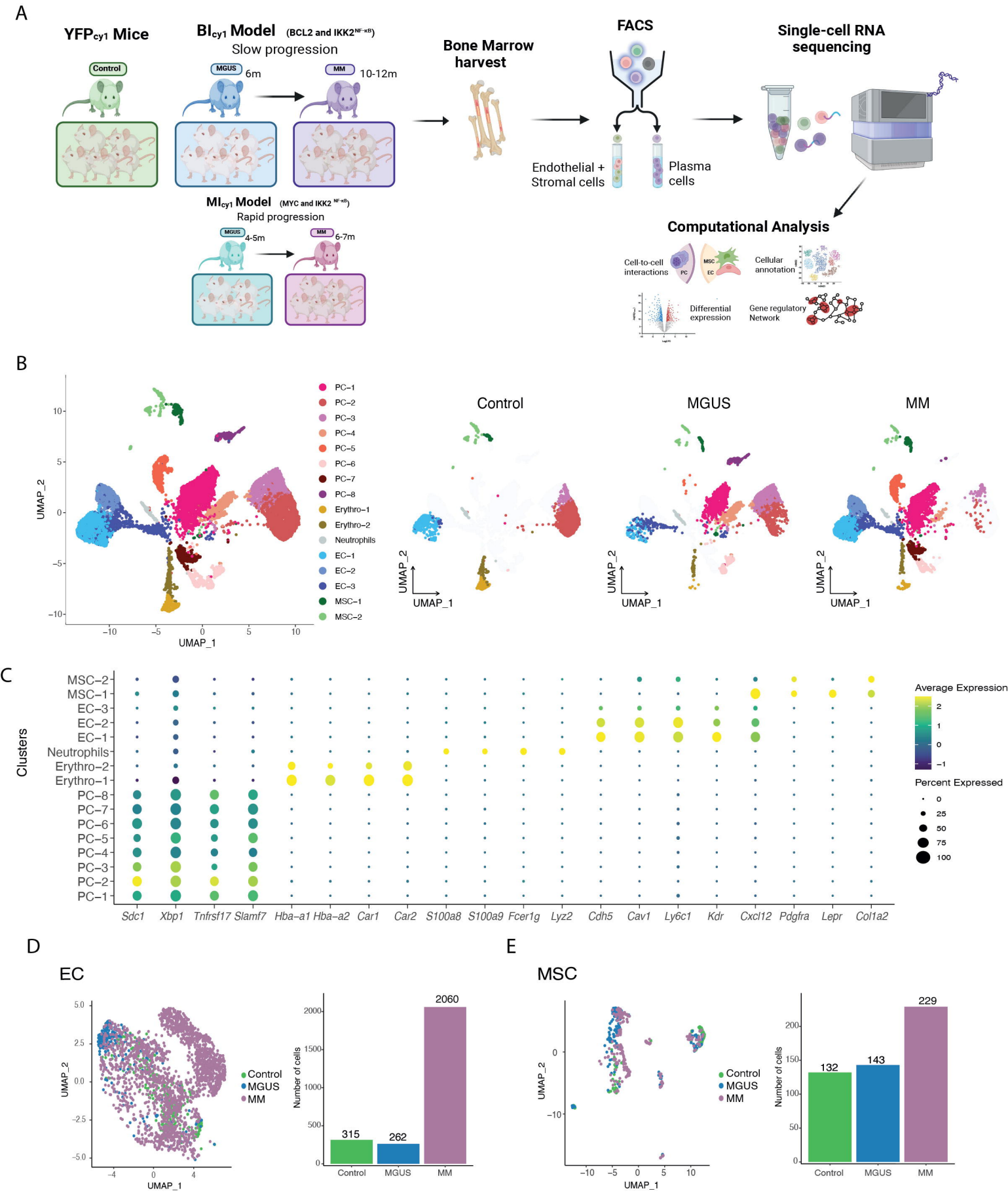
A
YFPcy1 Mice
Control
BIcy1 Model (BCL2 and IKK2NF-κB)
Slow progression
MGUS
6m
MM
10-12m
MIcy1 Model (MYC and IKK2 NF-κB)
Rapid progression
MGUS
4-5m
MM
6-7m
Bone Marrow harvest
FACS
Endothelial + Stromal cells
Plasma cells
Single-cell RNA sequencing
Computational Analysis
Cell-to-cell interactions
Cellular annotation
Differential expression
Gene regulatory Network
B
PC−1
PC−2
PC−3
PC−4
PC−5
PC−6
PC−7
PC−8
Erythro−1
Erythro−2
Neutrophils
EC−1
EC−2
EC−3
MSC−1
MSC−2
UMAP_1
UMAP_2
Control
MGUS
MM
C
Clusters
Average Expression
Percent Expressed
Sdc1
Xbp1
Tnfrsf17
Slamf7
Hba−a1
Hba−a2
Car1
Car2
S100a8
S100a9
Fcer1g
Lyz2
Cdh5
Cav1
Ly6c1
Kdr
Cxcl12
Pdgfra
Lepr
Col1a2
D
EC
Control
MGUS
MM
Number of cells
315
262
2060
E
MSC
132
143
229

FIGURE 2

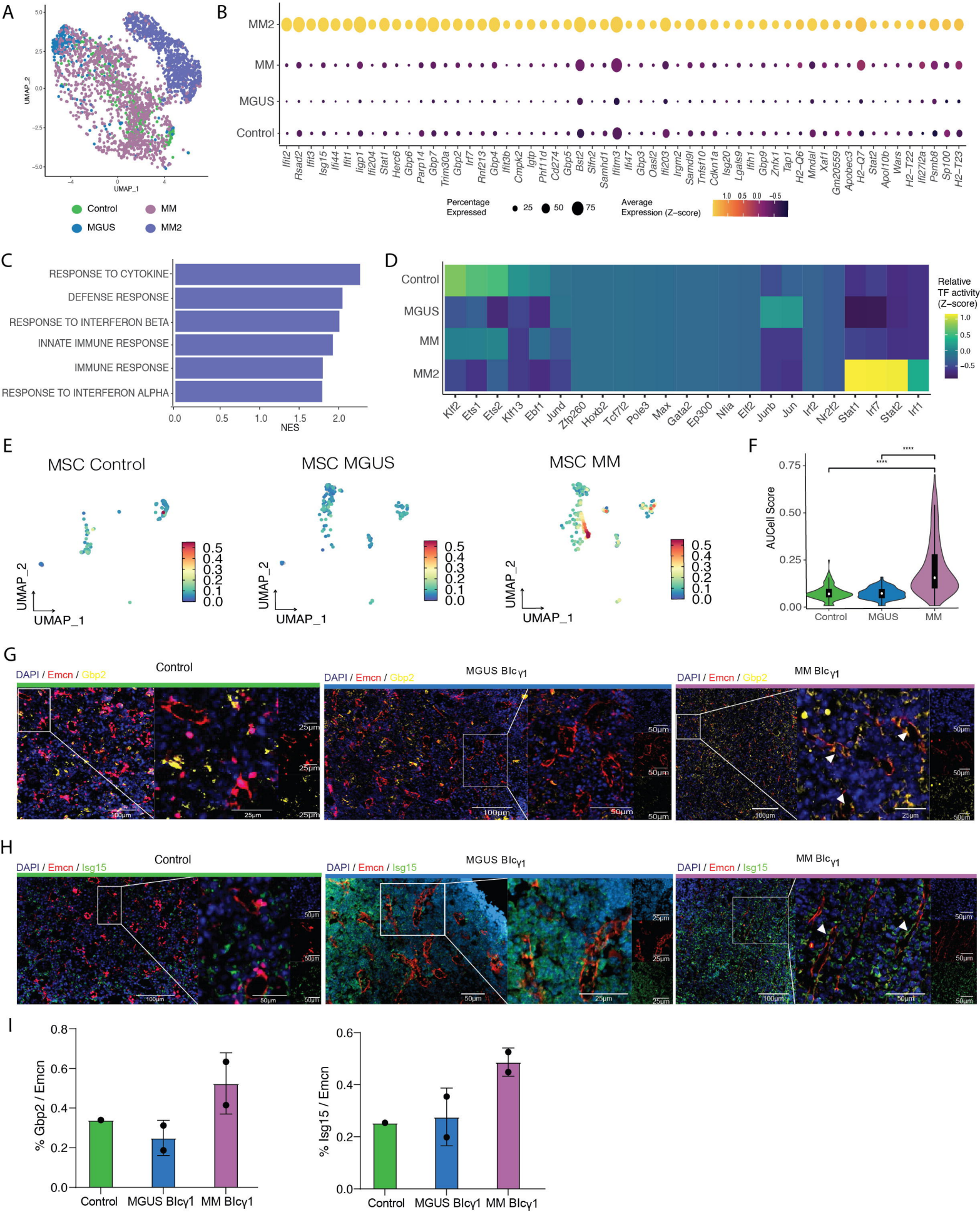
A
UMAP_2
UMAP_1
Control
MM
MGUS
MM2
B
MM2
MM
MGUS
Control
Ifit2 Rsad2 Ifit3 Isg15 Ifi44 Ifit1 Iigp1 Ifi204 Stat1 Herc6 Gbp6 Parp14 Gbp7 Trim30a Gbp2 Irf7 Rnf213 Gbp4 Ifit3b Cmpk2 Igtp Phf11d Cd274 Gbp5 Bst2 Slfn2 Samhd1 Ifitm3 Ifi47 Gbp3 Oasl2 Ifi203 Irgm2 Samd9l Tnfsf10 Cdkn1a Isg20 Lgals9 Ifih1 Gbp9 Znfx1 Tap1 H2-Q6 Mndal Xaf1 Gm20559 Apobec3 H2-Q7 Stat2 Apol10b Wars H2-T22 Ifi27l2a Psmb8 Sp100 H2-T23
Percentage Expressed
25
50
75
Average Expression (Z-score)
1.0 0.5 0.0 -0.5
C
RESPONSE TO CYTOKINE
DEFENSE RESPONSE
RESPONSE TO INTERFERON BETA
INNATE IMMUNE RESPONSE
IMMUNE RESPONSE
RESPONSE TO INTERFERON ALPHA
0.0 0.5 1.0 1.5 2.0
NES
D
Control
MGUS
MM
MM2
Klf2 Ets1 Ets2 Klf13 Ebf1 Jund Zfp260 Hoxb2 Tcf7l2 Pole3 Max Gata2 Ep300 Nfia Elf2 Junb Jun Irf2 Nr2f2 Stat1 Irf7 Stat2 Irf1
Relative TF activity (Z-score)
1.0
0.5
0.0
-0.5
E
MSC Control
MSC MGUS
MSC MM
UMAP_2
UMAP_1
0.5
0.4
0.3
0.2
0.1
0.0
F
AUCell Score
0.75
0.50
0.25
0.00
****
Control
MGUS
MM
G
Control
MGUS BIcγ1
MM BIcγ1
DAPI / Emcn / Gbp2
100µm
25µm
50µm
H
Control
MGUS BIcγ1
MM BIcγ1
DAPI / Emcn / Isg15
100µm
50µm
25µm
I
% Gbp2 / Emcn
0.8
0.6
0.4
0.2
0.0
Control
MGUS BIcγ1
MM BIcγ1
% Isg15 / Emcn
0.6
0.4
0.2
0.0
Control
MGUS BIcγ1
MM BIcγ1

FIGURE 3

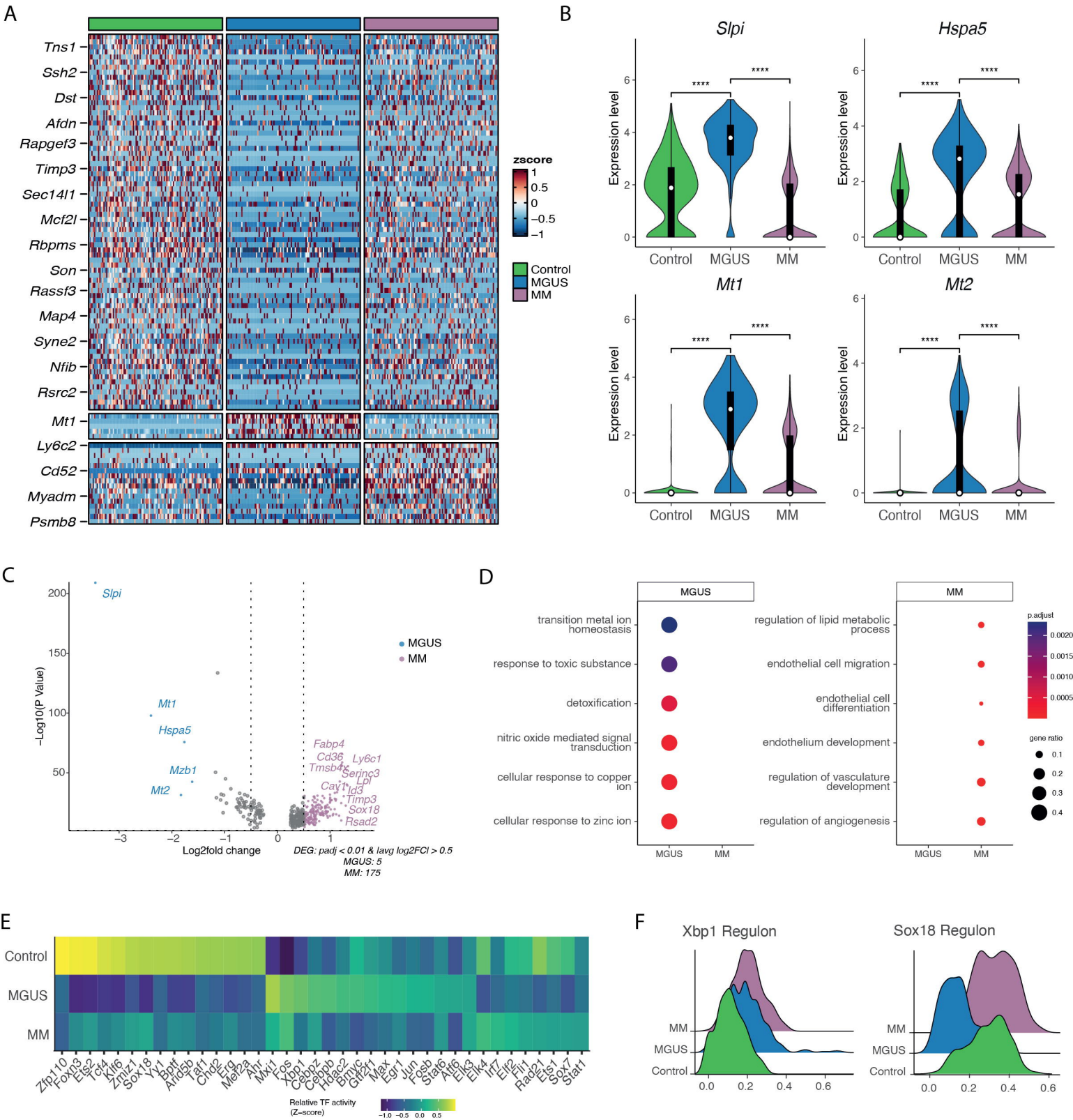
A
Tns1
Ssh2
Dst
Afdn
Rapgef3
Timp3
Sec14l1
Mcf2l
Rbpms
Son
Rassf3
Map4
Syne2
Nfib
Rsrc2
Mt1
Ly6c2
Cd52
Myadm
Psmb8
zscore
1
0.5
0
−0.5
−1
Control
MGUS
MM
B
Slpi
Hspa5
Mt1
Mt2
Expression level
Control
MGUS
MM
****
C
Slpi
Mt1
Hspa5
Mzb1
Mt2
Fabp4
Cd36
Tmsb4x
Ly6c1
Serinc3
Lpl
Cav1
Id3
Timp3
Sox18
Rsad2
MGUS
MM
−Log10(P Value)
Log2fold change
DEG: padj < 0.01 & lavg log2FCl > 0.5
MGUS: 5
MM: 175
D
MGUS
MM
transition metal ion homeostasis
response to toxic substance
detoxification
nitric oxide mediated signal transduction
cellular response to copper ion
cellular response to zinc ion
regulation of lipid metabolic process
endothelial cell migration
endothelial cell differentiation
endothelium development
regulation of vasculature development
regulation of angiogenesis
p.adjust
gene ratio
E
Control
MGUS
MM
Zfp110
Foxn3
Ets2
Tcf4
Klf6
Zmiz1
Sox18
Yy1
Bptf
Arid5b
Taf1
Chd2
Erg
Mef2a
Ahr
Mxi1
Fos
Xbp1
Cebpz
Cebpb
Hdac2
Bmyc
Gtf2f1
Max
Egr1
Jun
Fosb
Stat6
Atf6
Elk3
Elk4
Irf7
Elf2
Fli1
Rad21
Ets1
Sox7
Stat1
Relative TF activity
(Z-score)
F
Xbp1 Regulon
Sox18 Regulon
MM
MGUS
Control

FIGURE 4

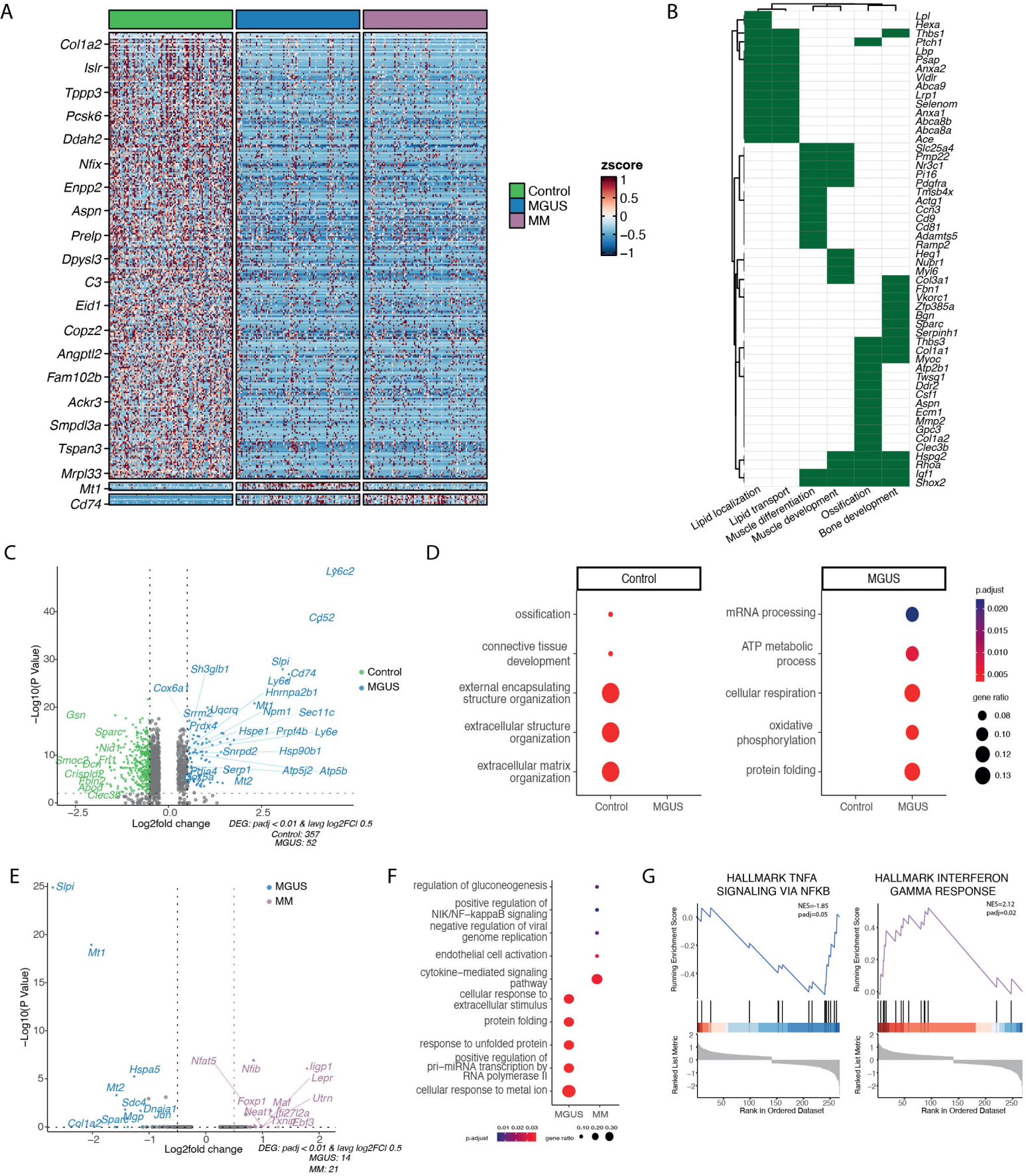
A
Col1a2
Islr
Tppp3
Pcsk6
Ddah2
Nfix
Enpp2
Aspn
Prelp
Dpysl3
C3
Eid1
Copz2
Angptl2
Fam102b
Ackr3
Smpdl3a
Tspan3
Mrpl33
Mt1
Cd74
Control
MGUS
MM
zscore
1
0.5
0
−0.5
−1
B
Lipid localization
Lipid transport
Muscle differentiation
Muscle development
Ossification
Bone development
C
Log2fold change
−Log10(P Value)
DEG: padj < 0.01 & lavg log2FCl 0.5
Control: 357
MGUS: 52
D
Control
MGUS
ossification
connective tissue development
external encapsulating structure organization
extracellular structure organization
extracellular matrix organization
mRNA processing
ATP metabolic process
cellular respiration
oxidative phosphorylation
protein folding
p.adjust
gene ratio
E
MGUS
MM
Log2fold change
−Log10(P Value)
DEG: padj < 0.01 & lavg log2FCl 0.5
MGUS: 14
MM: 21
F
regulation of gluconeogenesis
positive regulation of NIK/NF−kappaB signaling
negative regulation of viral genome replication
endothelial cell activation
cytokine−mediated signaling pathway
cellular response to extracellular stimulus
protein folding
response to unfolded protein
positive regulation of pri−miRNA transcription by RNA polymerase II
cellular response to metal ion
MGUS
MM
p.adjust
gene ratio
G
HALLMARK TNFA SIGNALING VIA NFKB
NES=-1.85
padj=0.05
HALLMARK INTERFERON GAMMA RESPONSE
NES=2.12
padj=0.02
Running Enrichment Score
Ranked List Metric
Rank in Ordered Dataset
H
Control
MGUS
MM
Relative TF activity (Z−score)
Clock (17g)
Hif1a (20g)
Creb3l2 (15g)
Ets2 (17g)
Myf5 (23g)
Yy1 (20g)
Xbp1 (15g)
Cux1 (11g)
Atf1 (23g)
Maff (15g)
Stat3 (18g)
Maz (14g)
Bmyc (15g)
Ctcf (18g)
Cebpd (25g)
Jund (40g)
Junb (38g)
Jun (36g)
Fos (18g)
Atf3 (16g)
Egr1 (37g)
Fosb (16g)
Dlx5 (11g)
Ar (17g)
Cebpa (40g)
Mef2c (30g)
Sox8 (28g)
Klf4 (183g)
Prrx2 (29g)
Sp7 (20g)
Sox9 (66g)
Klf2 (15g)
Mxd4 (23g)
Sp1 (20g)
Nr3c1 (12g)
Elk3 (31g)
Foxn3 (12g)
Zbtb7a (12g)
Ets1 (11g)
Rxra (23g)
Irf7 (11g)
Esr1 (15g)
Zmiz1 (25g)
Zeb1 (20g)
Nr2f6 (17g)
Hcfc1 (20g)
Hoxc10 (12g)
Ep300 (11g)
Brf2 (26g)

FIGURE 5

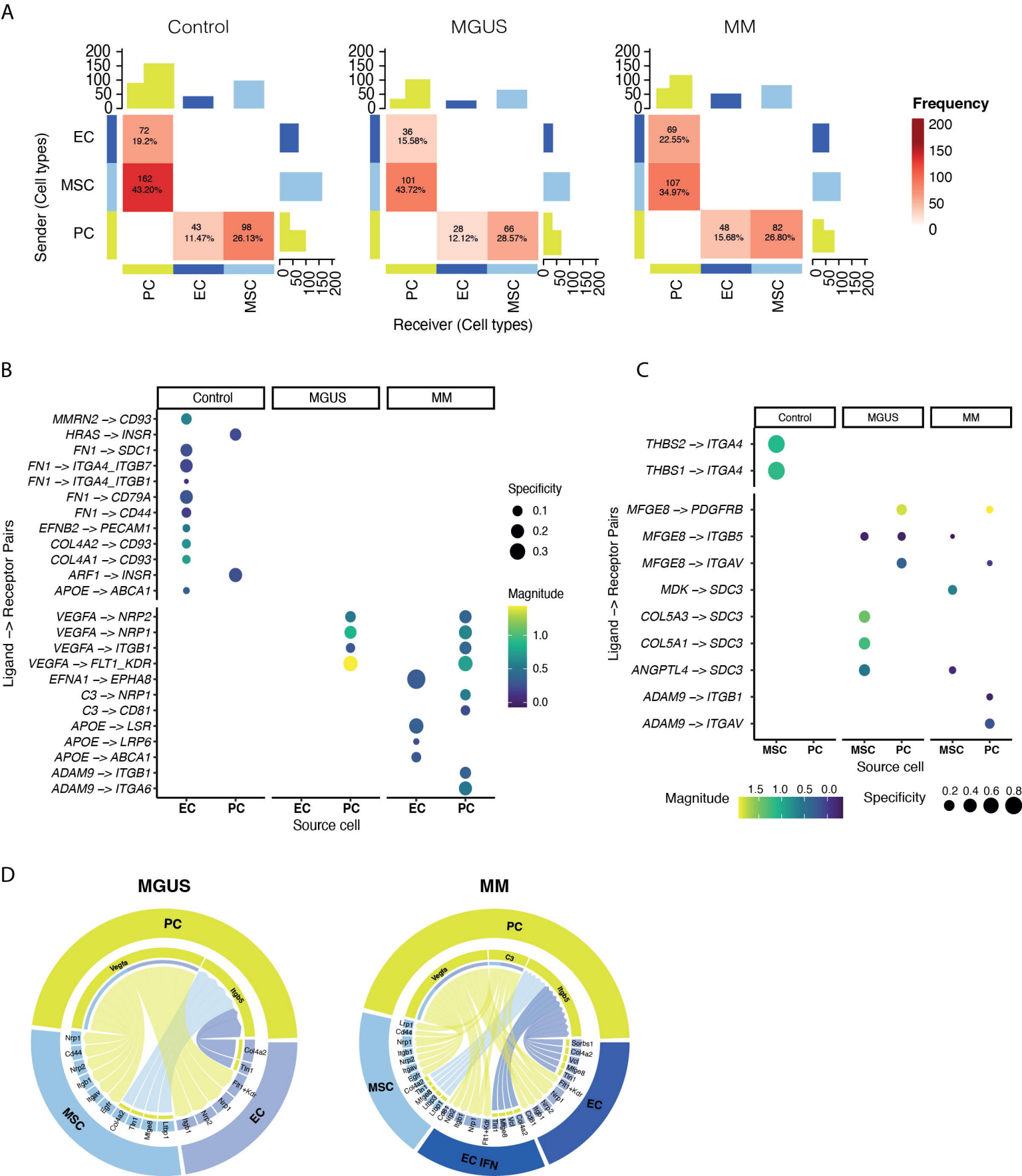
A
Control
MGUS
MM
Frequency
Sender (Cell types)
Receiver (Cell types)
EC
MSC
PC
72 19.2%
162 43.20%
43 11.47%
98 26.13%
36 15.58%
101 43.72%
28 12.12%
66 28.57%
69 22.55%
107 34.97%
48 15.68%
82 26.80%
B
Control
MGUS
MM
Ligand –> Receptor Pairs
MMRN2 –> CD93
HRAS –> INSR
FN1 –> SDC1
FN1 –> ITGA4_ITGB7
FN1 –> ITGA4_ITGB1
FN1 –> CD79A
FN1 –> CD44
EFNB2 –> PECAM1
COL4A2 –> CD93
COL4A1 –> CD93
ARF1 –> INSR
APOE –> ABCA1
VEGFA –> NRP2
VEGFA –> NRP1
VEGFA –> ITGB1
VEGFA –> FLT1_KDR
EFNA1 –> EPHA8
C3 –> NRP1
C3 –> CD81
APOE –> LSR
APOE –> LRP6
APOE –> ABCA1
ADAM9 –> ITGB1
ADAM9 –> ITGA6
Specificity
Magnitude
Source cell
C
Control
MGUS
MM
Ligand –> Receptor Pairs
THBS2 –> ITGA4
THBS1 –> ITGA4
MFGE8 –> PDGFRB
MFGE8 –> ITGB5
MFGE8 –> ITGAV
MDK –> SDC3
COL5A3 –> SDC3
COL5A1 –> SDC3
ANGPTL4 –> SDC3
ADAM9 –> ITGB1
ADAM9 –> ITGAV
Source cell
Magnitude
Specificity
D
MGUS
MM
PC
MSC
EC
EC IFN

FIGURE 6

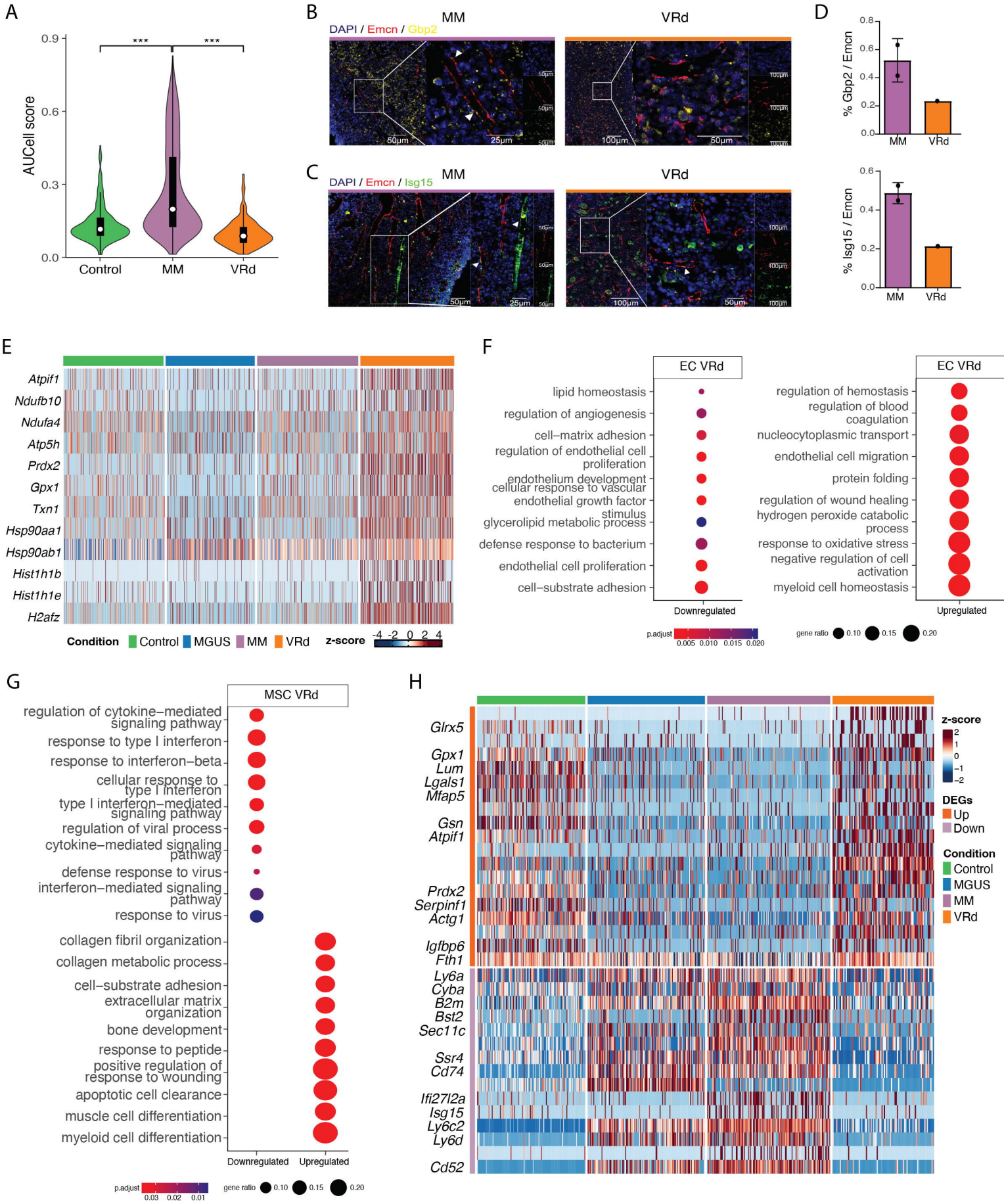
A
AUCell score
0.9
0.6
0.3
0.0
***
***
Control
MM
VRd
B
MM
VRd
DAPI / Emcn / Gbp2
50µm
25µm
100µm
C
MM
VRd
DAPI / Emcn / Isg15
D
% Gbp2 / Emcn
% Isg15 / Emcn
E
Atpif1
Ndufb10
Ndufa4
Atp5h
Prdx2
Gpx1
Txn1
Hsp90aa1
Hsp90ab1
Hist1h1b
Hist1h1e
H2afz
Condition
Control
MGUS
MM
VRd
z-score
-4 -2 0 2 4
F
EC VRd
lipid homeostasis
regulation of angiogenesis
cell–matrix adhesion
regulation of endothelial cell proliferation
endothelium development
cellular response to vascular endothelial growth factor stimulus
glycerolipid metabolic process
defense response to bacterium
endothelial cell proliferation
cell–substrate adhesion
Downregulated
regulation of hemostasis
regulation of blood coagulation
nucleocytoplasmic transport
endothelial cell migration
protein folding
regulation of wound healing
hydrogen peroxide catabolic process
response to oxidative stress
negative regulation of cell activation
myeloid cell homeostasis
Upregulated
p.adjust
0.005 0.010 0.015 0.020
gene ratio
0.10 0.15 0.20
G
MSC VRd
regulation of cytokine–mediated signaling pathway
response to type I interferon
response to interferon–beta
cellular response to type I interferon
type I interferon–mediated signaling pathway
regulation of viral process
cytokine–mediated signaling pathway
defense response to virus
interferon–mediated signaling pathway
response to virus
collagen fibril organization
collagen metabolic process
cell–substrate adhesion
extracellular matrix organization
bone development
response to peptide
positive regulation of response to wounding
apoptotic cell clearance
muscle cell differentiation
myeloid cell differentiation
Downregulated
Upregulated
p.adjust
0.03 0.02 0.01
gene ratio
0.10 0.15 0.20
H
Glrx5
Gpx1
Lum
Lgals1
Mfap5
Gsn
Atpif1
Prdx2
Serpinf1
Actg1
Igfbp6
Fth1
Ly6a
Cyba
B2m
Bst2
Sec11c
Ssr4
Cd74
Ifi27l2a
Isg15
Ly6c2
Ly6d
Cd52
z-score
2
1
0
−1
−2
DEGs
Up
Down
Condition
Control
MGUS
MM
VRd

FIGURE 7

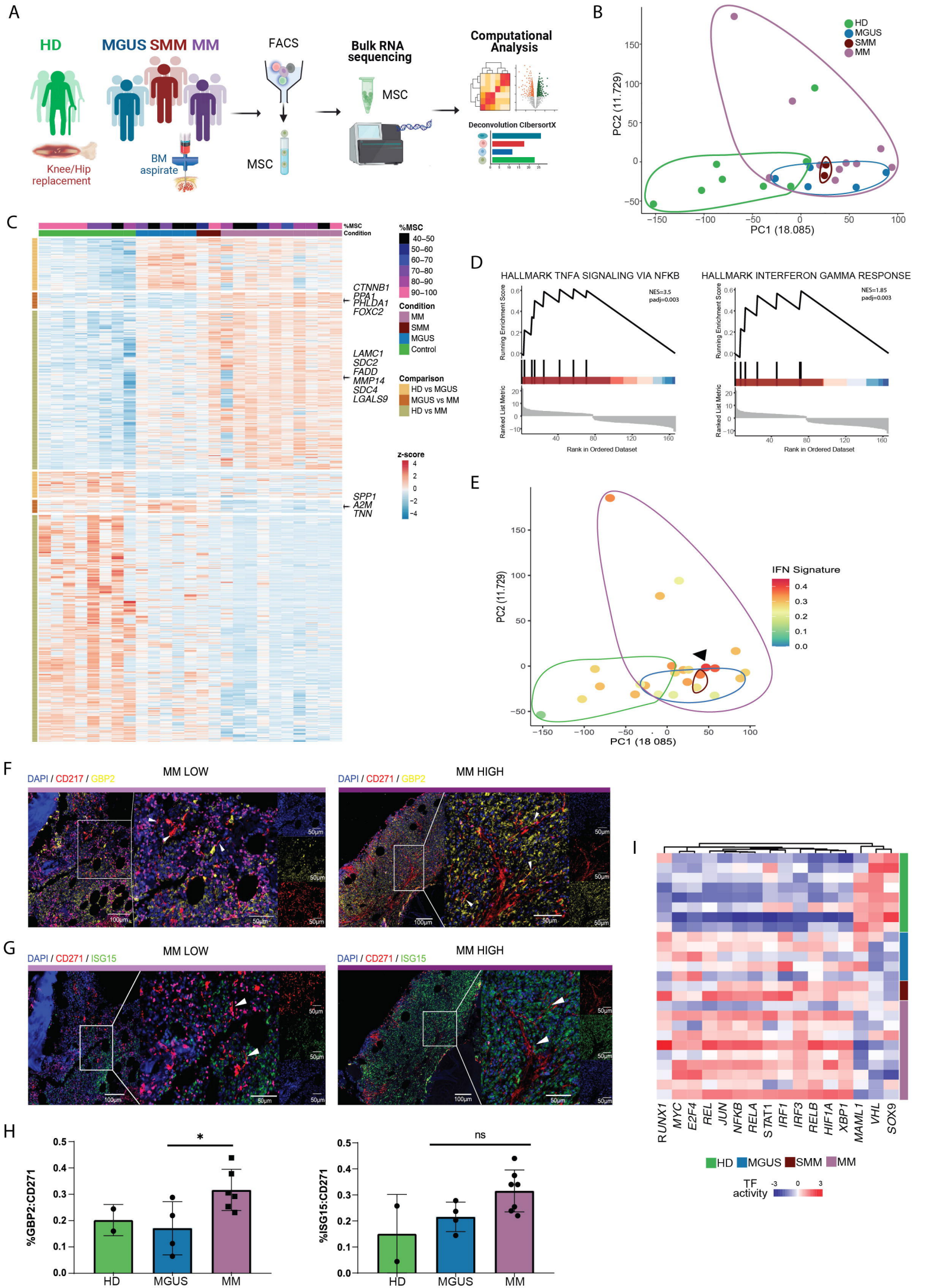
A
HD
MGUS SMM MM
Knee/Hip replacement
BM aspirate
FACS
MSC
Bulk RNA sequencing
MSC
Computational Analysis
Deconvolution CIbersortX
B
HD
MGUS
SMM
MM
PC2 (11.729)
PC1 (18.085)
C
%MSC
Condition
%MSC
40–50
50–60
60–70
70–80
80–90
90–100
Condition
MM
SMM
MGUS
Control
Comparison
HD vs MGUS
MGUS vs MM
HD vs MM
z-score
CTNNB1
PPA1
PHLDA1
FOXC2
LAMC1
SDC2
FADD
MMP14
SDC4
LGALS9
SPP1
A2M
TNN
D
HALLMARK TNFA SIGNALING VIA NFKB
NES=3.5
padj=0.003
HALLMARK INTERFERON GAMMA RESPONSE
NES=1.85
padj=0.003
Running Enrichment Score
Ranked List Metric
Rank in Ordered Dataset
E
IFN Signature
PC2 (11.729)
PC1 (18 085)
F
MM LOW
DAPI / CD217 / GBP2
MM HIGH
DAPI / CD271 / GBP2
G
MM LOW
DAPI / CD271 / ISG15
MM HIGH
DAPI / CD271 / ISG15
H
%GBP2:CD271
*
HD
MGUS
MM
%ISG15:CD271
ns
I
RUNX1
MYC
E2F4
REL
JUN
NFKB
RELA
STAT1
IRF1
IRF3
RELB
HIF1A
XBP1
MAML1
VHL
SOX9
HD MGUS SMM MM
TF activity